Dynamic spin structure factor of $SrCu_2(BO_3)_2$ at finite temperatures

S. El Shawish,[1] J. Bonča,[1,2] and I. Sega[1]
[1]*J. Stefan Institute, SI-1000 Ljubljana, Slovenia*
[2]*Faculty of Mathematics and Physics, University of Ljubljana, SI-1000 Ljubljana, Slovenia*
(Received 2 March 2005; revised manuscript received 23 August 2005; published 7 November 2005)

Using finite temperature Lanczos technique on finite clusters we calculate dynamical spin structure factor of the quasi-two-dimensional dimer spin liquid $SrCu_2(BO_3)_2$ as a function of wave vector and temperature. At low temperatures the peak belonging to the lowest spin excitations is split due to spin anisotropy, in accord with the experimental data. Unusual temperature dependence of calculated spectra is as well in agreement with inelastic neutron scattering measurements. Normalized peak intensities of the single-triplet peak are **q** independent, their temperature dependence is analyzed in terms of thermodynamic quantities.

DOI: 10.1103/PhysRevB.72.184409 PACS number(s): 75.10.Jm, 75.40.Gb, 75.40.Mg, 75.25.+z

I. INTRODUCTION

In low-dimensional quantum spin systems quantum fluctuations often lead to disordered ground states that exhibit no magnetic ordering and a gapped, nondegenerate singlet ground state. Such states, also called spin liquids, are realized in one dimension in dimerized or frustrated spin chains, even-leg spin ladders as well as in the two-dimensional Shastry-Sutherland (SHS) model.[1] $SrCu_2(BO_3)_2$ is a quasi-two-dimensional spin system with a unique spin-rotation invariant exchange topology that leads to a singlet dimer ground state.[2] Since this compound represents the only known realization of the SHS model, it recently became a focal point of theoretical as well as experimental investigations in the field of frustrated spin systems. Consequently, many fascinating physical properties of $SrCu_2(BO_3)_2$ have been discovered. Increasing external magnetic field leads to a formation of magnetization plateaus[3,4] which are a consequence of repulsive interaction between almost localized triplets. Weak anisotropic spin interactions can have disproportionately strong effect in a frustrated system. It has recently been shown, that the inclusion of the nearest neighbor (NN) and next-nearest neighbor (NNN) Dzyaloshinsky-Moriya (DM) interactions is required to explain some qualitative features of the specific heat near the transition from the spin dimer to the spin-triplet state, as well as to explain the low frequency lines observed in electron spin resonance experiments in $SrCu_2(BO_3)_2$.[5–11]

While there is a general agreement that the SHS model with addition of DM terms adequately describes zero-temperature static and dynamic properties of $SrCu_2(BO_3)_2$,[11,12] as well as thermodynamic properties, e.g., the uniform static spin susceptibility and specific heat at finite magnetic fields,[8] there still remain open problems concerning the temperature dependence of dynamic properties of the system. The existence of the spin gap, almost localized spin-triplet excited states, as well as the proximity of a spin-liquid ground state of $SrCu_2(BO_3)_2$ to the ordered antiferromagnetic state, lead to rather unusual low-temperature properties emerging in inelastic neutron scattering (INS),[13,14] Raman scattering (RS)[15] as well as in electron spin resonance (ESR) experiments.[7] In particular, INS normalized peak intensities of single-, double-, and possibly triple-modes show a rapid decrease with temperature around 13 K, well below the value of the spin gap energy $\Delta \sim 34$ K. In addition, the authors of Ref. 14 show, that properly normalized complement of static uniform spin susceptibility, obtained with almost identical model parameters as in the present work,[8] nearly perfectly fits their experimental data. Similar behavior is found in RS data where a dramatic decrease of Raman modes, representing transitions between the ground state and excited singlets, with increasing temperature at $T \ll \Delta$ is observed. Moreover, at $T \sim \Delta$ all RS modes become strongly overdamped.[15]

Numerical simulations of dynamical spin structure factor based on exact diagonalization on small clusters at zero temperature show good agreement with INS data.[12] Recently developed zero-temperature method based on perturbative continuous unitary transformations[16,17] gives very reliable results for the dynamical spin structure factor of the SHS model since the method does not suffer from finite-size effects. The method is, however, limited to calculations at zero temperature and, at least at the present stage, it does not allow for the inclusion of DM terms.

The aim of this work is to investigate finite temperature properties of the dynamical spin structure factor of the SHS model using the finite temperature Lanczos method (FTLM),[18,19] and to compare results with INS data.[13,14] We show, that unusual temperature dependence of INS data can be adequately explained using the SHS model. In our search for deeper physical understanding of spectral properties of the SHS model at finite temperatures we compare these with thermodynamic quantities, such as the specific heat, and uniform static magnetic susceptibility, which we further compare with analytical results of the isolated dimer (DIM) model. We finally present results of the **q**-dependent static magnetic susceptibility as a function of T.

II. MODEL AND METHOD

To describe the low-temperature properties of $SrCu_2(BO_3)_2$ we consider the following Heisenberg Hamiltonian defined on a two-dimensional (2D) Shastry-Sutherland lattice:[1]

$$H_s = J\sum_{\langle \mathbf{i},\mathbf{j}\rangle} \mathbf{S_i}\cdot\mathbf{S_j} + J'\sum_{\langle \mathbf{i},\mathbf{j}\rangle'} \mathbf{S_i}\cdot\mathbf{S_j} + \sum_{\langle \mathbf{i}\to\mathbf{j}\rangle'} \mathbf{D}'\cdot(\mathbf{S_i}\times\mathbf{S_j}). \quad (1)$$

Here, $\langle \mathbf{i},\mathbf{j}\rangle$ and $\langle \mathbf{i},\mathbf{j}\rangle'$ indicate that $\mathbf{i}$ and $\mathbf{j}$ are NN and NNN, respectively. A recently presented high-resolution INS measurments on $SrCu_2(BO_3)_2$ (Ref. 14) motivated us to choose $J=76.8$ K (in units of k_B) and $J'/J=0.62$. A slightly different choice of parameters ($J=74.0$ K, $J'/J=0.62$) has been used previously in describing specific heat measurements[8] and ESR experiments on $SrCu_2(BO_3)_2$.[11] We should note, however, that this small change of parameters leads to effects visible only on small energy scales, thus leaving previous calculations[8,11] practically unaffected. In addition to the Shastry-Sutherland Hamiltonian, H_s includes DM interactions to NNN with the corresponding DM vector $\mathbf{D}'$. The arrows indicate that bonds have a particular orientation as described in Ref. 8. Its value, $\mathbf{D}'=1.77$ K $\hat{\mathbf{z}}$, successfully explains the splitting between the two single-triplet excitations observed in ESR[5,7] and INS measurements.[13,14]

As pointed out in Refs. 8 and 11, a finite NN DM term should also be taken into account to explain specific heat data and ESR experiments. We have chosen to omit this term since it does not significantly affect results of the dynamical spin structure factor at a nonzero value of the wave vector. We have chosen the quantization axis $\hat{\mathbf{z}}$ to be parallel to the c axis and $\hat{\mathbf{x}}$ to the a axis pointing along the centers of neighboring parallel dimers.

We use the FTLM based on the Lanczos procedure of exact diagonalization, combined with random sampling over initial wave functions. For a detailed explaination of the method and a definition of method parameters see Refs. 18 and 19. All the results are computed on a tilted square lattice of $N=20$ sites with $M_1=100$ first and $M_2=250$ second Lanczos steps, respectively. The full trace summation over $N_{st}=2^N\sim 10^6$ states is replaced by a much smaller set of $R\sim 10^3$ random states giving the sampling ratio $R/N_{st}\sim 10^{-3}$. In order to estimate the finite-size effects we have also performed calculations on a 16-site cluster.

Comparing FTLM with the conventional quantum Monte Carlo (QMC) methods we emphasize the following advantages: (a) the absence of the minus-sign problem that usually hinders QMC calculations of frustrated spin systems, (b) the method connects the high- and low-temperature regimes in a continuous fashion, and (c) dynamic properties can be calculated straightforwardly in the real time in contrast to employing the analytical continuation from the imaginary time, necessary when using QMC calculations. Among the shortcomings of FTLM is its limitation to small lattices that leads to the appearance of finite-size effects as the temperature is lowered below a certain $T<T_{fs}$. Due to the existence of the gap in the excitation spectrum and the almost localized nature of the lowest triplet excitation, we estimate $T_{fs}\sim 1$ K at least for calculation of thermodynamic properties.[8] Finite-size effects also affect dynamical properties as, e.g., the dynamical spin structure factor, which is (even at finite temperatures) represented as a set of delta functions. In particular, finite-size effects affect the frequency resolution at low temperatures, while at higher temperatures as more states contribute to the spectra, its shape becomes less size dependent.

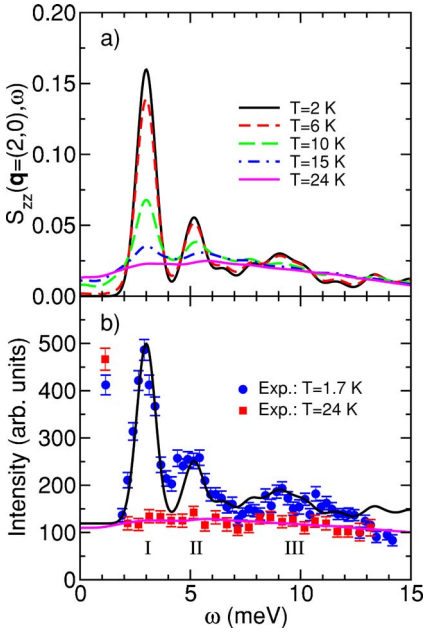

FIG. 1. (Color online) (a) Spin structure factor $S_{zz}(\mathbf{q},\omega)$ for $\mathbf{q}=(2,0)$ where $\mathbf{q}$ is given in units of the reciprocal lattice vectors (Ref. 21) vs ω for different values of T, and (b) comparison with INS measurements from Ref. 13. Transitions to single-, double-, and triple-triplet states are indicated with Roman numerals. Parameters of the model are $J=76.8$ K, $J'=47.6$ K, $D_z'=1.77$ K. We use units where $\hbar=1$.

We should stress that FTLM was in the past successfully used in obtaining thermodynamic as well as dynamic properties of different correlated models as are the t-J model,[18,19] the Hubbard model,[20] as well as the SHS model.[8]

III. NUMERICAL RESULTS AND COMPARISON WITH EXPERIMENT

A. Dynamical spin structure factor

For comparison with the INS data, we compute the dynamical spin structure factor for $\mu=x,y,z$,

$$S_{\mu\mu}(\mathbf{q},\omega) = \mathrm{Re}\int_0^\infty dt e^{i\omega t}\langle S^\mu_{\mathbf{q}}(t)S^\mu_{-\mathbf{q}}(0)\rangle,$$

$$S^\mu_{\mathbf{q}} = \frac{1}{\sqrt{N}}\sum_{i,\alpha} S^\mu(\mathbf{R}_i+\mathbf{r}_\alpha)e^{i\mathbf{q}(\mathbf{R}_i+\mathbf{r}_\alpha)}, \quad (2)$$

where i runs over all unit cells of the lattice and $\mathbf{r}_\alpha$ spans four vectors forming the basis of the unit cell that contains two orthogonal dimers. For the details describing interatomic distances we refer the reader to Ref. 16. The average in Eq. (2) represents the thermodynamic average which is computed using FTLM.[18]

In Fig. 1(a) we first present the spin structure factor $S_{zz}(\mathbf{q},\omega)$ for different temperatures. We should note that due

to a finite value $D_z'=1.77$ K spin rotational invariance of the Hamiltonian, Eq. (1), is broken, i.e., $S_{xx}(\mathbf{q},\omega)=S_{yy}(\mathbf{q},\omega) \neq S_{zz}(\mathbf{q},\omega)$. Since $D_z' \ll J,J'$, the effect of broken symmetry is, at least within our numerical precision, negligible for energy resolutions much larger than the value of anisotropic interaction, $\Delta\omega \gg D_z'$, yielding nearly identical results for the three components $\mu=x,y$, and z of $S_{\mu\mu}(\mathbf{q},\omega)$. Since the spectra consist of a set of delta functions, we have artificially broadened the peaks with a Gaussian form with $\sigma=0.4$ meV, to achieve the best fit with INS measurements.[13] Two peaks (I and II) are clearly visible at low temperatures $T=2$ K $\ll\Delta$ around $\omega\sim 3$ meV and 5 meV, associated with transitions to single- and bound double-triplet states.[13] A broader peak (III) around $\omega=9$ meV can be interpreted as correlated three-triplet or multitriplet excitations.[13] Results at $T=2$ K are consistent with previous $T=0$ simulations.[12,16] Increasing temperature has a pronounced effect on $S_{zz}(\mathbf{q},\omega)$, manifesting in a rapid decrease of $S_{zz}(\mathbf{q},\omega)$ with temperature, at temperatures even far below the value of the gap. Quantitatively, at $T=24$ K the peak structure almost completely disappears. In Fig. 1(b) we present comparison of our numerical data scaled and shifted along the vertical axis to compensate for experimental background for two different temperatures along with experimental values from Ref. 13.

In order to investigate magnetic anisotropy effects, originating from the finite DM term D_z', one has to turn to high-energy resolution calculations with frequency precision comparable to the magnitude of the DM interaction. On this frequency scale we expect to find substancial difference between longitudinal and transverse components of the spin structure factor. For this reason we have included the transverse component of the spin structure factor according to the relation for the differential cross section

$$\frac{d^2\sigma}{d\Omega d\omega} \propto \sum_{\mu\nu}\left(\delta_{\mu\nu}-\frac{q_\mu q_\nu}{q^2}\right)S_{\mu\nu}(\mathbf{q},\omega). \tag{3}$$

For a given direction of the neutron momentum transfer, e.g., $\mathbf{q}=(-2,0)$ as used to obtain high-resolution INS data presented in Fig. 2(b), Eq. (3) reduces to a sum of the transverse and longitudinal part, $d^2\sigma/d\Omega d\omega \propto S_{yy}(\mathbf{q},\omega)+S_{zz}(\mathbf{q},\omega)$. In Fig. 2(a) we first present the temperature dependence of $d^2\sigma/d\Omega d\omega$. The main effect of increasing temperature is seen as a decrease in the spectral weight, while the three-peak structure remains visible up to temperatures as high as $T=24$ K. The main reason that this structure is not smeared by the increasing temperatures lies in the fact, that the three-peak structure emerges due to transitions from the ground state to the in-gap narrow-band single-triplet states.

To describe the origin of the three-peak structure in more detail, we present in Fig. 2(b) both contributions to the differential cross section in Eq. (3) as well as their sum, plotted against the high-resolution INS data.[14] The best fit is achieved for $J=76.8$ K, $J'=47.6$ K, $D_z'=1.77$ K, and artificial broadening of the Gaussian form with $\sigma=0.05$ meV. The outer two modes represent transitions between the ground state and two $S_z=\pm 1$ single-triplet excitations that are split due to finite value of D_z'. These two transitions are proportional to $S_{yy}(\mathbf{q},\omega)$. The actual splitting $\Delta\sim 0.32$ meV between the outer two modes yields $4D_z'/\Delta\sim 1.9$ for the renormalization of the bandwidth due to quantum fluctuations. This is as well in agreement with the estimate of Cepas *et al.*[5] The middle peak represents the transition between the ground state and the excited, doubly degenerate $S_z=0$ triplet state, induced by $S_{zz}(\mathbf{q},\omega)$. Note, that the position of the latter peak is not affected by D_z'.[5]

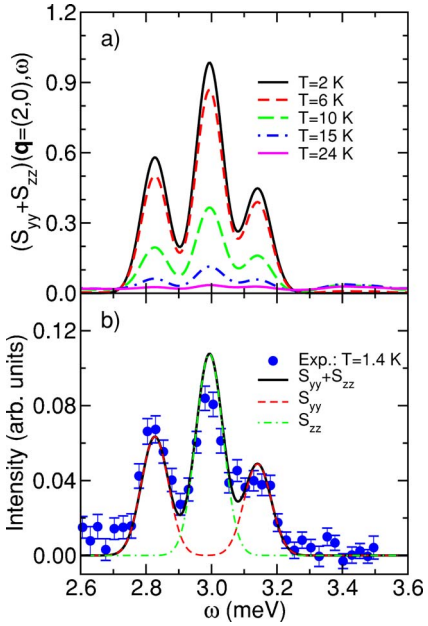

FIG. 2. (Color online) (a) Sum of the transverse $S_{yy}(\mathbf{q},\omega)$ and longitudinal $S_{zz}(\mathbf{q},\omega)$ contributions of a single-triplet mode for different values of T, and (b) comparison with the high-resolution data for $\mathbf{q}=(-2,0)$ and $T=1.4$ K from Ref. 14. Parameters of the model are identical to those of Fig. 1.

In Fig. 3 we present a map of $S_{zz}(\mathbf{q},\omega)$ for different temperatures. Peak I with almost no dispersion is clearly visible at $\omega\sim 3$ meV with its highest intensity located near $q_x\sim 2$. Peak II, located at $\omega\sim 5$ meV is also visible and similarly shows little dispersion. Its intensity is as well maximal near $q_x\sim 2$. Note that due to a small system size $S_{zz}(\mathbf{q},\omega)$ plots were calculated at only a few discrete values of q_x, i.e., $q_x=0.0$, 1.0, 2.0, and 3.0. The geometry of the tilted square lattice with $N=20$ sites excludes half-integer values of q_x. This fact prevents us to directly compare our intensity plot results for the spin structure factor with the ones shown in Ref. 14, where the dispersion of the lowest triplet mode, attributed mainly to the transverse part of the spin structure factor, is clearly seen. We have calculated the transverse component $S_{yy}(\mathbf{q},\omega)$ but since it does not differ considerably from $S_{zz}(\mathbf{q},\omega)$ on a given energy scale we do not present it in Fig. 3. Note, that a map, shown in Fig. 3, was obtained by interpolation between allowed integer values of q_x. These results are roughly consistent with measurements by Gaulin *et al.*[14] With increasing T peaks I and II rapidly decrease (more quantitative analysis of the temperature dependence follows in the next section), while visible response due to elastic transitions among identical multiplets starts developing around $\omega=0$ and $q_x=0$.

For comparison we also present the analytic expression for $S_{zz}(\mathbf{q},\omega)$ of the simplistic DIM model with $J=\Delta=34$ K,

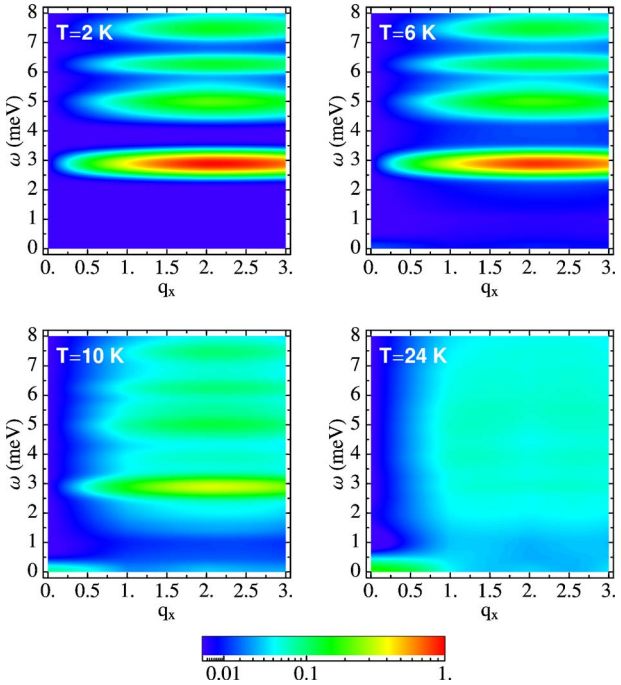

FIG. 3. (Color online) Intensity plot of the spin structure factor $S_{zz}(\mathbf{q},\omega)$ in the q_x-ω plane for different values of T as indicated in the figures. The intensity scale is logarithmic and $\sigma=0.2$ meV is used to broaden the spectra as a function of frequency ω.

where J is chosen in such a way that SHS and DIM models share identical energy gaps between the singlet ground state and the excited triplet state. In the latter case analytical expression for $S_{zz}(\mathbf{q},\omega)$ can be straightforwardly derived

$$S_{zz}(\mathbf{q},\omega) = \pi A(\mathbf{q})[\delta(\omega - J) + e^{-\beta J}\delta(\omega + J)] + 2\pi B(\mathbf{q})e^{-\beta J}\delta(\omega) \tag{4}$$

with $A(\mathbf{q})$ and $B(\mathbf{q})$ given by

$$A(\mathbf{q}) = \frac{\sin^2 \eta(q_x - q_y) + \sin^2 \eta(q_x + q_y)}{4(1 + 3e^{-\beta J})}, \tag{5}$$

$$B(\mathbf{q}) = \frac{\cos^2 \eta(q_x - q_y) + \cos^2 \eta(q_x + q_y)}{4(1 + 3e^{-\beta J})}, \tag{6}$$

and $\eta=0.717$. [Note also that in the limit $T\to\infty$ $\int_{-\infty}^{\infty} S_{zz}(\mathbf{q},\omega)d\omega=\pi/4$.] At $T=0$ $S_{zz}(\mathbf{q},\omega)$ consists of a single delta function at $\omega=J$ weighted by $A(\mathbf{q})$.[13] This peak corresponds to peak I in the SHS model with its $\mathbf{q}$ dependence approximately given by $A(\mathbf{q})$. Note also that peaks II and III do not have their counterparts in $S_{zz}(\mathbf{q},\omega)$ of the simplistic DIM model. With increasing T peaks at $\omega=-J$ and $\omega=0$ appear, weighted by $\pi A(\mathbf{q})\exp(-\beta J)$ and $2\pi B(\mathbf{q})\exp(-\beta J)$, respectively. Further comparison of the above analytical result for $S_{zz}(\mathbf{q},\omega)$ with the SHS model shows, that the peak at $\omega=0$ that emerges with increasing T is as well clearly seen in the SHS model (see Fig. 3).

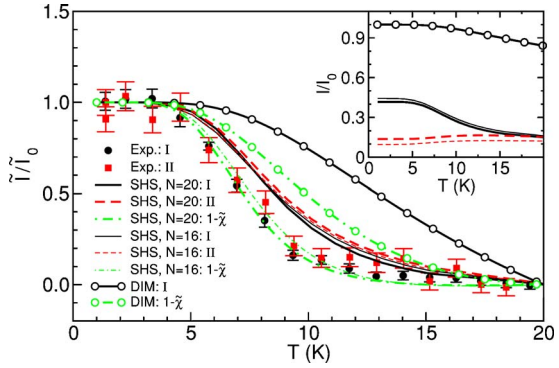

FIG. 4. (Color online) Normalized peak intensities $\tilde{I}/\tilde{I}_0$ of peaks I and II vs T from Ref. 14 (filled symbols). FTLM results of $\tilde{I}/\tilde{I}_0$ as well as $1-\tilde{\chi}$, calculated using the $N=20$ cluster are presented with thick lines and those using the $N=16$ cluster with thin lines. Results for the DIM model are presented with open circles connected with lines. The inset, relative integrated intensities I/I_0 of peaks I and II. Parameters of the model are identical to those of Fig. 1.

B. Normalized peak intensities

With the purpose to further quantify the agreement of our calculations with the experiment we present in Fig. 4 the normalized peak intensities $\tilde{I}/\tilde{I}_0$ of the two peaks (I and II) as functions of temperature along with the measured data taken from Ref. 14. To avoid contributions from the background at higher temperatures, peak intensities were measured from their values at $T=20$ K,

$$\tilde{I}/\tilde{I}_0 = \frac{S_{zz}(\mathbf{q},\omega_P,T) - S_{zz}(\mathbf{q},\omega_P,20\text{ K})}{S_{zz}(\mathbf{q},\omega_P,0) - S_{zz}(\mathbf{q},\omega_P,20\text{ K})}, \tag{7}$$

with $\omega_P=3.0$ meV and $\omega_P=5.0$ meV for peaks I and II, respectively. Gaussian broadening with $\sigma=0.4$ meV was used to obtain peak values of $S_{zz}(\mathbf{q},\omega_P,T)$. A similar temperature behavior is observed as in INS measurements,[13,14] manifesting itself in a rapid decrease of both peak intensities with temperature for T far below the gap value $\Delta=34$ K. Taking this fact into account, the agreement between experimental values and numerical calculations of $\tilde{I}/\tilde{I}_0$ is reasonable even though not ideal. However, as already suggested by Gaulin *et al.*,[14] nearly perfect agreement between experiment and rescaled complement of the uniform static susceptibility $1-\tilde{\chi}=1-\chi_0(T)/\chi_0(T=20\text{ K})$ is found where $\chi_0=\langle (S^z_{\text{tot}})^2\rangle/NT$, and S^z_{tot} represents the z component of the total spin. We were unable to find a direct analytical connection between the two quantities, i.e., $1-\tilde{\chi}$ and $\tilde{I}/\tilde{I}_0$. In Fig. 4 both quantities are presented for comparison. Furthermore, analytical calculations of $1-\tilde{\chi}$ and $\tilde{I}/\tilde{I}_0$ on the DIM model, as well presented in Fig. 4, also point to a different T dependence. This leads us to the conclusion, that nearly perfect agreement with $1-\tilde{\chi}$ and experimental results of Ref. 14 may be accidental.

A slight disagreement of numerical and experimental results of $\tilde{I}/\tilde{I}_0$ can be in part attributed to finite-size effects. A thorough finite-size analysis is not possible due to a limited number of available lattice sizes. Nevertheless, to obtain at least a rough estimate of the finite-size effects, we present in

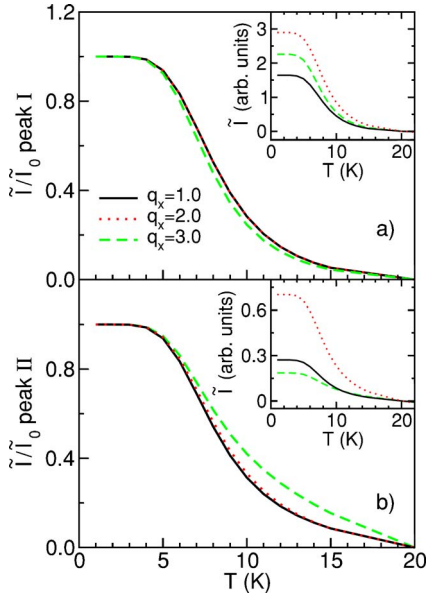

FIG. 5. (Color online) Normalized peak intensities $\tilde{I}/\tilde{I}_0$ of peaks (a) I and (b) II vs T calculated at different values of $\mathbf{q}=(q_x,0)$. In insets unrenormalized peak intensities measured from the peak intensity position at $T=20$ K are shown.

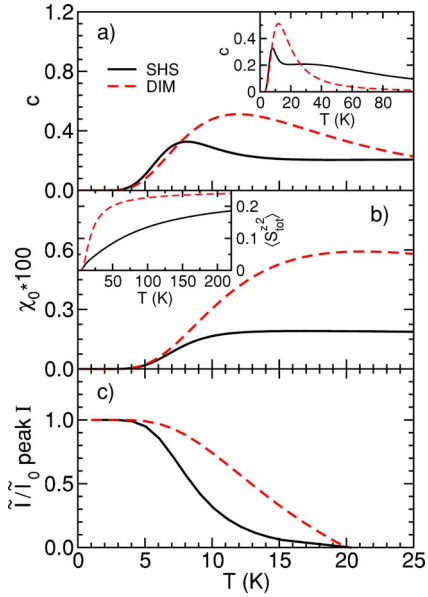

FIG. 6. (Color online) Thermodynamic properties of the SHS model on $N=20$-site system (full lines) and DIM model with $J=34$ K (dashed lines), (a) specific heat c vs T (insets represents c in the expanded temperature range) and (b) uniform static susceptibility χ_0 vs T ($\langle S^z_{\rm tot}{}^2\rangle$ in the inset). For completeness and to facilitate comparison we present in (c) normalized peak intensity $\tilde{I}/\tilde{I}_0$ of peak I vs T measured from values at $T=20$ K as shown in Fig. 4. Parameters of the model are identical to those in Fig. 1.

Fig. 4 along with results for the $N=20$ system, as well those for the $N=16$ system. Comparison of different results suggests, that finite-size effects are rather small and furthermore, that finite-size effects of $\tilde{I}/\tilde{I}_0$, derived from the dynamical correlation function $S_{zz}(\mathbf{q},\omega)$ are comparable (or even slightly smaller) with those of $1-\tilde{\chi}$, representing a static quantity.

In the inset of Fig. 4 we show the integrated intensities of the two peaks defined as $I(\omega_1,\omega_2)/I_0 = \int_{\omega_1}^{\omega_2} d\omega S_{zz}(\mathbf{q},\omega)/\langle S_{\mathbf{q}}S_{-\mathbf{q}}\rangle$ where the limits of integration defining integrated peak intensities are defined as follows: $I_{\rm I} = I(2\text{ meV},4\text{ meV})$ and $I_{\rm II}=I(4\text{ meV},6\text{ meV})$ for peaks I and II, respectively. We observe a distinctive difference in temperature behavior between $I_{\rm I}/I_0$ on the one hand and $I_{\rm II}/I_0$ on the other. While $I_{\rm I}/I_0$ substantially decreases with increasing temperature similarly to $\tilde{I}/\tilde{I}_0$, indicating on a considerable shift of the spectral weight away from transition I, $I_{\rm II}/I_0$ shows even a slight temperature increase. We suggest that this difference is caused by a different nature of the transition from the ground state to the localized triplet (peak I) in contrast to transitions to states near or else within continuum. Furthermore, the temperature dependence of $I_{\rm I}/I_0$ mimics that of the DIM model. This behavior is as well in agreement with INS measurements[13] that show peak I being only resolution limited while peaks II and III show intrinsic linewidths.

We now explore the $\mathbf{q}$ dependence of peak intensities. In Fig. 5 we present normalized values of peak intensities vs T for various values of q_x at fixed $q_y=0$ and find nearly perfect scaling of $\tilde{I}/\tilde{I}_0$ for peak I, Fig. 5(a), while scaling breaks down at $q_x=3.0$ for peak II, Fig. 5(b). Such behavior is characteristic also for the simpler DIM model that possesses a single temperature scale J. This result suggests that a single temperature scale is responsible for the T dependence of peak I for all different values of $\mathbf{q}$. In the insets of Figs. 5(a) and 5(b) we present absolute values of peak intensities for different values of q_x. Intensities of both peaks I and II reach their maximum values at low T near $q_x\sim 2.0$. Taking into account our rather poor resolution in the q_x space, we find these results to be roughly consistent with recent high-resolution INS measurements by Gaulin *et al.*[14]

C. Thermodynamic properties

Next, we will connect the spectral data with thermodynamic properties of the Hamiltonian defined in Eq. (1). For this reason we present in Fig. 6(a) the specific heat (per spin) $c=T(\partial s/\partial T)=(\langle H^2\rangle-\langle H\rangle^2)/NT^2$, where N is the number of spins in the system. A low T peak in c is located well below the value of the gap, i.e., at $T=T_1\sim 8.0$ K$=0.24\Delta$. In the inset of Fig. 6(a) c is shown in an expanded T interval where it can be clearly seen that the peak at $T=T_1$ is followed by a broader peak located at $T=T_2\sim 30$ K$=0.39J$. While the first peak, centered at T_1, arises from the in-gap narrow-band states in the spectrum of H, the rather broad second peak is due to excitations in the continuum. Its peak position is of the order of J, the highest energy scale in the system. For comparison, in the pure Heisenberg model c displays only a single-peak structure where the peak position is at $T\sim 0.6J$.[22]

Note that c, obtained using the same method and for slightly different values of J, J' and $\mathbf{D}'$, apart for additional DM terms, fits measured specific heat data of $SrCu_2(BO_3)_2$ in a wide range of applied external magnetic fields.[8] We

should furthermore stress that the influence of DM terms on all quantities presented in Fig. 6 is negligible. Their effect on thermodynamic properties becomes more relevant when applying a large external magnetic field.[8] For comparison we also present c of the DIM model with $J=\Delta=34$ K that can be solved analytically. DIM model shows a simple Schottky-type behavior, see Fig. 6(a), which clearly differs from the peak-shoulder structure of $c(T)$ observed in the SHS model. We should point out, however, that even in a simple DIM model c peaks well below the gap value, i.e., at $T=T_1\sim 11.9$ K$=0.35\Delta$.

In Fig. 6(b) we present the uniform static spin susceptibility, χ_0. While comparison of χ_0 with experimental data was presented elsewhere,[8] in this work we present it along with other thermodynamic properties just to gain a more complete physical picture of the temperature dependence of $S_{zz}(\mathbf{q},\omega)$. The steepest increase in χ_0 vs T coincides with the peak in c and, at least approximately, with the steepest decrease of $\tilde{I}/\tilde{I}_0$, presented in Fig. 4, see also Fig. 6(c). At low temperatures $\chi_0(T\lesssim 5\text{ K})\sim 0$, where the temperature interval $T\lesssim 5$ K in turn corresponds to the plateau of $\tilde{I}/\tilde{I}_0$ seen in experimental results of peaks I and II as well as in our numerical simulations.

We have tested the robustness of thermodynamic properties presented in Fig. 6 against finite-size effects by computing identical properties on the $N=16$ system. Results of c, $\langle S^z_{\text{tot}}{}^2\rangle$, and χ_0 on the $N=16$ system differ by less than the presented linewidths.

We would like to make some general remarks on comparing thermodynamic properties of the SHS model and the DIM model with identical gaps between the ground state and first excited states. Such a direct comparison may assist in understanding the influence of spin frustration and the proximity of gapless excitations in the SHS model on its thermodynamic properties. In particular, the specific heat c of the SHS model peaks at lower temperature than c of the DIM model and shows two maxima in contrast to a single, Schottky-type maximum seen in the DIM model. And finally, the peak value of χ_0 is almost three times lower in the SHS model than in the DIM model which in turn implies that spin fluctuations, $\langle S^z_{\text{tot}}{}^2\rangle$ [see the inset of Fig. 6(b)], of the SHS model are suppressed in comparison to the DIM model.

D. Static spin susceptibility $\chi(\mathbf{q})$

Finally, we present in Fig. 7 the static spin susceptibility

$$\chi(\mathbf{q})=\frac{1}{\pi}\mathcal{P}\int_{-\infty}^{\infty}\frac{\chi''(\mathbf{q},\omega)}{\omega}d\omega, \tag{8}$$

$$\chi''(\mathbf{q},\omega)=(1-e^{-\beta\omega})\mathbf{S}_{zz}(\mathbf{q},\omega), \tag{9}$$

as a function of $\mathbf{q}=(q_x,0)$. Besides fulfilling theoretical interest, $\chi(\mathbf{q})$ can also be used to compute, e.g., spin-spin nuclear relaxation rate $1/T_2$. Along $\chi(\mathbf{q})$ of the SHS model we present for comparison results for the DIM model where the analytical result can be readily obtained using Eqs. (4), (8), and (9),

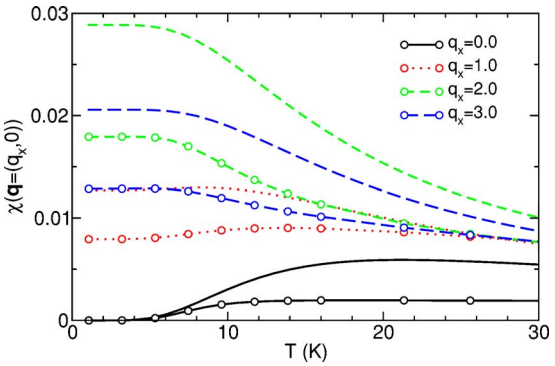

FIG. 7. (Color online) $\chi[\mathbf{q}=(q_x,0)]$ vs T for several values of q_x. Circles connected with lines present results of the SHS model, lines present results of the DIM model, Eq. (10) with $J=34$ K.

$$\chi(\mathbf{q})=2A(\mathbf{q})(1-e^{-\beta J})/J+2B(\mathbf{q})e^{-\beta J}\beta, \tag{10}$$

where $A(\mathbf{q})$ and $B(\mathbf{q})$ are defined in Eqs. (5) and (6). At low T, i.e., $T\lesssim 5$ K, $\chi(\mathbf{q})$ vs T is nearly T independent which is a consequence of the spin gap. As a function of q_x it reaches its maximum value near $q_x\sim 2.0$ in accord with the prediction of the DIM model result, Eq. (10). Observed T dependence is again similar to the DIM model prediction. At higher temperatures, i.e., $T\gtrsim 300$ K, $\chi(\mathbf{q})$ merges with universal, $\mathbf{q}$-independent form, i.e., $\chi(\mathbf{q})=1/4T$.

IV. CONCLUSIONS

In conclusion, we have computed dynamical spin structure factor at finite temperatures. Frequency dependence of $S_{zz}(\mathbf{q},\omega)$ at $T=2$ K and 24 K agree reasonably well with INS measurements[13] on a large energy scale. High-resolution INS data for the lowest triplet excitation[14] is as well almost perfectly captured by calculated transverse and longitudinal components, $S_{yy}(\mathbf{q},\omega)+S_{zz}(\mathbf{q},\omega)$, showing the influence of anisotropy present in the system and simultaneously setting the energy scale for D'_z, i.e., $D'_z=1.7$ K. Apart from explaining the three-peak structure in high-resolution INS data, the DM term has due to its small value in comparison with other parameters of the system almost no effect on thermodynamic properties at zero magnetic field.

Temperature dependence of the normalized peak intensities $\tilde{I}/\tilde{I}_0$ agrees well with INS measurements[13,14] that show a rather unexpected drop of peak intensities with increasing temperature, at temperatures well below the value of the energy gap. We have thus shown, that the SHS model successfully describes temperature dependence of dynamic properties of the $SrCu_2(BO_3)_2$ system at low temperatures. We attribute a minor disagreement between measured data and numerical simulations to finite-size effects.

Our calculations predict that $\tilde{I}/\tilde{I}_0$ of peak I should be $\mathbf{q}$ independent. Such behavior is in agreement with the DIM model prediction for peak I, while peak II is anyhow absent in this simplistic model. Our results are thus consistent with a proposition that a single temperature scale is responsible for the T dependence of peak I for all different values of $\mathbf{q}$. This statement does not take into account a possible small

dispersion of peak I due to DM interaction or (and) due to high-order processes in J'/J.[12] From comparison of temperature dependence of $\tilde{I}/\tilde{I}_0$ with thermodynamic properties it is obvious that strong T dependence of $\tilde{I}/\tilde{I}_0$, occurring well below the value of the spin gap, is in accord with strong T dependence of other thermodynamic properties. The temperature of the steepest decrease of $\tilde{I}/\tilde{I}_0$ coincides with the peak in c and the steepest increase of χ_0.

There is obviously a need for further, less finite-size dependent calculations that will clarify many unanswered questions as are, e.g., the role of DM terms in explaining small dispersion of peaks I and II observed in high-resolution INS experiments,[14] an explanation of unusual temperature dependence of ESR lines[7] that seem to decrease in width as the temperature increases, the occurrence of magnetization plateaus, etc. Nevertheless, the main features of temperature-dependent dynamic properties of the SHS model seem to be well captured by the FTLM on small lattices which is in turn reflected in a good agreement with experiments.

ACKNOWLEDGMENTS

The authors acknowledge inspiring discussions with C. D. Batista and B. D. Gaulin that took place during the preparation of this paper. The authors also acknowledge the financial support of Slovene Research Agency under Contract No. P1-0044.

[1] B. S. Shastry and B. Sutherland, Physica D **108**, 1069 (1981).
[2] R. W. Smith and D. A. Keszler, J. Solid State Chem. **93**, 430 (1991).
[3] H. Kageyama, K. Yoshimura, R. Stern, N. V. Mushnikov, K. Onizuka, M. Kato, K. Kosuge, C. P. Slichter, T. Goto, and Y. Ueda, Phys. Rev. Lett. **82**, 3168 (1999).
[4] K. Onizuka, H. Kageyama, Y. Narumi, K. Kindo, Y. Ueda, and T. Goto, J. Phys. Soc. Jpn. **69**, 1016 (2000).
[5] O. Cépas, K. Kakurai, L. P. Regnault, T. Ziman, J. P. Boucher, N. Aso, M. Nishi, H. Kageyama, and Y. Ueda, Phys. Rev. Lett. **87**, 167205 (2001).
[6] O. Cépas, T. Sakai, and T. Ziman, Prog. Theor. Phys. Suppl. **145**, 43 (2002).
[7] H. Nojiri, H. Kageyama, Y. Ueda, and M. Motokawa, J. Phys. Soc. Jpn. **72**, 3243 (2003).
[8] G. A. Jorge, R. Stern, M. Jaime, N. Harrison, J. Bonča, S. E. Shawish, C. D. Batista, H. A. Dabkowska, and B. D. Gaulin, Phys. Rev. B **71**, 092403 (2005).
[9] A. Zorko, D. Arčon, H. Kageyama, and A. Lappas, Appl. Magn. Reson. **27**, 267 (2004).
[10] A. Zorko, D. Arčon, H. van Tol, L. C. Brunel, and H. Kageyama, Phys. Rev. B **69**, 174420 (2004).
[11] S. El Shawish, J. Bonča, C. D. Batista, and I. Sega, Phys. Rev. B **71**, 014413 (2005).
[12] S. Miyahara and K. Ueda, J. Phys.: Condens. Matter **15**, R327 (2003).
[13] H. Kageyama, M. Nishi, N. Aso, K. Onizuka, T. Yosihama, K. Nukui, K. Kodama, K. Kakurai, and Y. Ueda, Phys. Rev. Lett. **84**, 5876 (2000).
[14] B. D. Gaulin, S. H. Lee, S. Haravifard, J. P. Castellan, A. J. Berlinsky, H. A. Dabkowska, Y. Qiu, and J. R. D. Copley, Phys. Rev. Lett. **93**, 267202 (2004).
[15] P. Lemmens, M. Grove, M. Fischer, G. Güntherodt, Valeri N. Kotov, H. Kageyama, K. Onizuka, and Y. Ueda, Phys. Rev. Lett. **85**, 2605 (2000).
[16] C. Knetter and G. S. Uhrig, Phys. Rev. Lett. **92**, 027204 (2004).
[17] K. P. Schmidt, C. Knetter, and G. S. Uhrig, Phys. Rev. B **69**, 104417 (2004).
[18] J. Jaklič and P. Prelovšek, Adv. Phys. **49**, 1 (2000).
[19] J. Jaklič and P. Prelovšek, Phys. Rev. Lett. **77**, 892 (1996); Phys. Rev. B **49**, 5065 (1994).
[20] J. Bonča and P. Prelovšek, Phys. Rev. B **67**, 085103 (2003).
[21] Definition of the wave vector **q** is identical to the one used in Refs. 13 and 16.
[22] M. S. Makivic and H.-Q. Ding, Phys. Rev. B **43**, 3562 (1991).